THE END-TO-END CONVECTIVE HAZARD RISK FORECAST PROCESS DEVELOPED BY THE AUSTRALIAN EXTREME WEATHER DESK FOR THE SOUTH AUSTRALIAN 28 SEPTEMBER 2016 TORNADO OUTBREAK

Dean Sgarbossa *
National Forecast Services
Bureau of Meteorology, Melbourne, Australia

Jonathon Fischer
National Forecast Services
Bureau of Meteorology, Adelaide, Australia

Matthew Bass
National Forecast Services
Bureau of Meteorology, Adelaide, Australia

James Taylor
National Forecast Services
Bureau of Meteorology, Melbourne, Australia

1. INTRODUCTION

During the afternoon and evening of 28 September 2016, one of the most significant severe thunderstorm outbreaks in recent decades impacted central and eastern parts of the Australian state of South Australia. Multiple supercell thunderstorms produced damaging to destructive wind gusts, including at least seven tornadoes, very large hailstones and locally intense rainfall. These supercell thunderstorms and tornadoes impacted the South Australian power network, contributing to a state-wide power outage leaving up to 1.7 million people (ABS 2018) without electricity.

A brief description and damage assessment for two tornadoes that caused damage to high-voltage electricity transmission lines is presented in section 2. The Australian Bureau of Meteorology National Forecast Services' Extreme Weather Desk (EWD) convective hazard risk forecast process is described in section 3 which stems from an amalgamation of best-practice guidance and continuous improvement through structured verification providing an end-to-end forecast process. The meteorology of this high-impact event is described on several scales in a cascading fashion, from the broad scale antecedent conditions and climate forcing mechanisms in section 4, through the synoptic-scale forcing in section 5, to the convective and mesoscale environments in sections 6 and 7 respectively. The performance of the EWD's national probabilistic thunderstorm forecasts are presented in section 8, along with additional post-event analysis including the comparison of conditional tornado probability assessment from RADAR and mesoanalysis to the tornado damage assessment.

* *Corresponding author address:* Dean Sgarbossa, Bureau of Meteorology, National Forecast Services, Extreme Weather Desk, GPO Box 1636 Melbourne VIC 3001, Australia;
e-mail: dean.sgarbossa@bom.gov.au

2. TORNADO DAMAGE ASSESSMENT

The tornado outbreak of 28 September 2016 was one of the most significant severe thunderstorm outbreaks to affect Australia in recent decades, consisting of multiple supercell thunderstorms associated with a quasi-linear convective system (QLCS) that impacted parts of South Australia's eastern and central areas, producing damaging to destructive wind gusts, very large hailstones, locally intense rainfall and at least seven tornadoes. The combination of intense wind gusts and tornadoes impacted the South Australian power network and contributed to a state-wide power outage that left up to 1.7 million people (ABS 2018) without electricity. Five faults which occurred within a period of 88 seconds led to the 'black system event' (AEMO 2016) which refers to an event that leads to a complete loss of power. Four of these faults occurred on three high-voltage transmission lines that are designed to withstand wind gusts up to 120 km h^{-1} (AEMO 2016), caused by the impact of tornadic supercell thunderstorms; two of the damaged transmission lines spaced over 100 km apart were damaged by two separate tornadoes within 88 seconds of each other (AEMO 2016 and AEMO 2017).

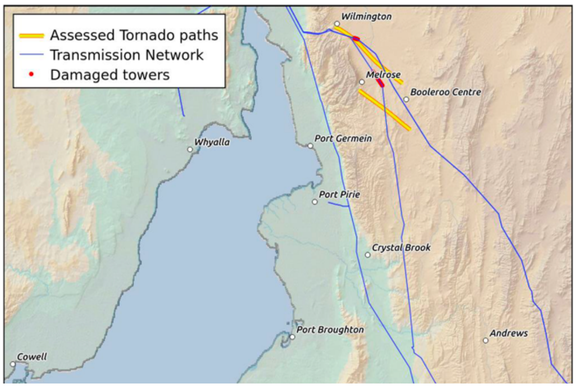

FIG 1. The locations of the four assessed tornado paths overlaid with the electricity transmission network (blue) and damaged towers (red).

Damage surveys were conducted for four of the seven identified tornadoes on 6 October 2016 (Figure 1) and included the capturing of photographic evidence which was used to estimate the path and intensity of the tornadoes (Bureau of Meteorology 2016b). All wind speed ranges given are estimates only based on the Enhanced Fujita/Fujita Scale of tornado damage. Damage was assigned an upper and lower bound of probable wind speeds using the damage indicators (DI) and degrees of damage (DOD) after McDonald and Mehta (2006) and assigned a rating from the Enhanced Fujita Scale. These ratings were then converted to the Fujita Scale (Fujita 1981) which is the standard tornado rating system used by the Bureau of Meteorology. It should be noted that the Enhanced Fujita Scale of tornado damage is based on human-built structures and vegetation in North America and as such, differences in construction standards and vegetation types increases the uncertainty of wind speed estimates.

Three of the tornadoes were assessed to have caused damage consistent with a F2 intensity rating (181–253 km h^{-1}), while the remaining assessed tornado with an estimated F1 (117–180 km h^{-1}) intensity rating. For brevity, only the two assessed tornadoes that caused damage to transmission lines are outlined below. Please refer to Bureau of Meteorology (2016b) report for full DI and DOD assessments for damage markers numbered in Figures 2 and 6.

2.1 *Blyth Tornado*

The Blyth tornado commenced to the north-northwest of the town of Blyth at approximately 06:05 UTC and tracked approximately 19 km towards the southeast through farms, native vegetation, residential properties and community buildings in the township of Blyth before ending to the south of the town of Kybunga at approximately 06:20 UTC[1] (Figure 2). A tower on the Brinkworth-Templers West transmission line had collapsed towards the northwest which was opposing the direction of storm motion (Figure 3); the damage sustained and timing was consistent with the location and timing of the electrical fault. The upper bound of wind speeds from the damage markers reached the low end of the F3 tornado intensity scale, but a lack of supportive evidence of this wind speed from other damage indicators excludes a rating beyond F2 and consequently, the tornado was rated an F2 (181–253 km h^{-1}) intensity rating.

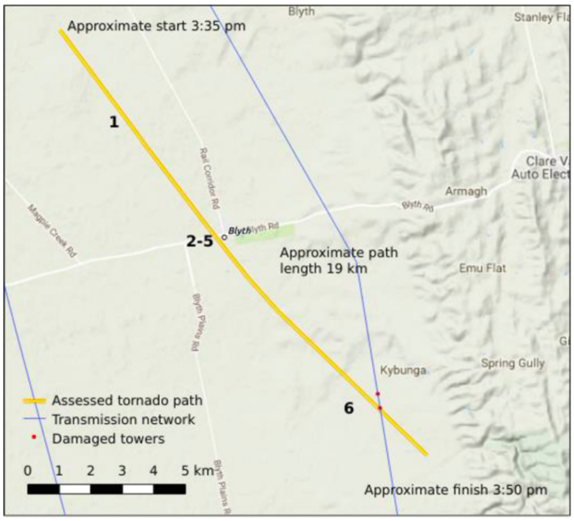

FIG 2. Approximate path of the Blyth tornado with damage markers numbered, electricity transmission network (blue) and damaged towers (red).

FIG 3. Blyth tornado damage marker 6; collapsed metal truss of a tower on the Brinkworth-Templers West transmission line.

[1] The state of South Australia observes Australian Central Standard Time which is 9:30 hours ahead of Coordinated Universal Time (UTC).

FIG 4. Blyth tornado damage marker 2; church hall full loss of roof.

FIG 5: Video still of Blyth tornado. Attribution: Jace Bourne.

2.2 *Wilmington tornado*

The Wilmington tornado commenced to the south of the town of Wilmington at approximately 06:15 UTC and tracked towards the southeast through a caravan park and across farms and native vegetation for an approximate distance of 30 km before weakening below tornadic strength 6 km north of the town of Booleroo at approximately 06:35 UTC (Figure 6). The upper bound of wind speeds from three damage markers reached the low end of the F3 tornado intensity scale, but a lack of supportive evidence of this wind speed from other damage indicators excludes a rating beyond F2 and consequently, the tornado was rated an F2 (181–253 km h^{-1}) intensity rating. Five towers on the Davenport – Belalie/Davenport - Mt Lock transmission lines were damaged (Figure 7) between 06:15 and 06:25 UTC by the tornado as supported by RADAR, video and damage survey evidence, the timing and location of which is consistent with the electrical faults on these lines between 06:17:59 and 06:18:14 UTC (AEMO 2016).

An additional 14 towers were damaged along the Davenport - Brinkworth transmission line by the supercell thunderstorm that produced the Wilmington tornado and were located well to the south of the Wilmington tornado damage path. Little evidence of significant damage to vegetation or structures was evident within the vicinity of the towers.

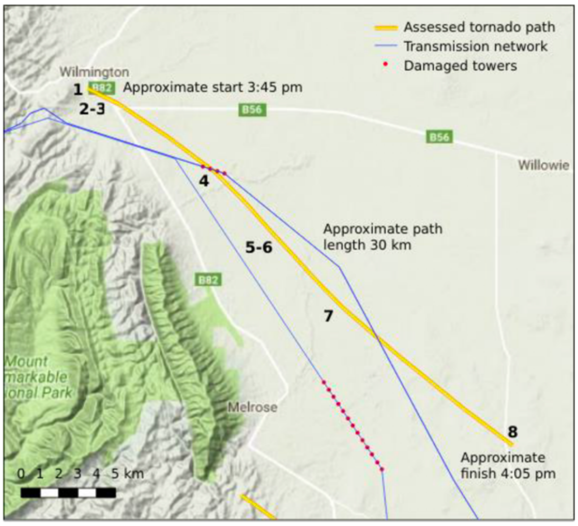

FIG 6. Approximate path of the Wilmington tornado with damage markers numbered, electricity transmission network (blue) and damaged towers (red).

FIG 7. Wilmington tornado damage marker 4; collapsed metal truss of a tower on the Davenport-Belalie/Davenport-Mt Lock transmission line.

FIG 8. Tornadic damage to trees along Spring Creek, indicating the approximate width of the Wilmington tornado.

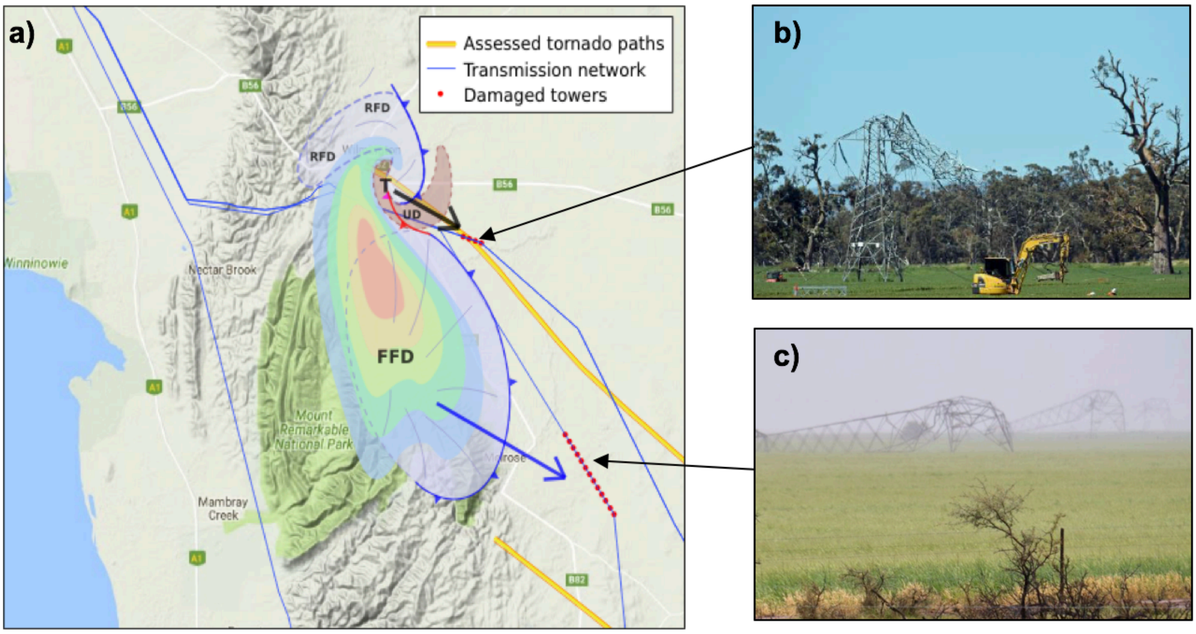

FIG 9. a) Idealised Wilmington, SA supercell thunderstorm, depicting the position of the tornado (T), forward flank downdraught (FFD), rear flank downdraught (RFD) and updraught (UD), and the impact on the b) Davenport-Belalie/Davenport-Mt Lock transmission line from the tornado; and c) Davenport-Brinkworth transmission line from the FFD.

When combined with RADAR evidence and the position and collapse orientation of the damaged towers (Figure 9c), it is suggested that the towers were impacted by straight-line winds associated with the forward flank downdraft of the supercell thunderstorm which may have been enhanced by the co-alignment with the storm motion (Figure 9a).

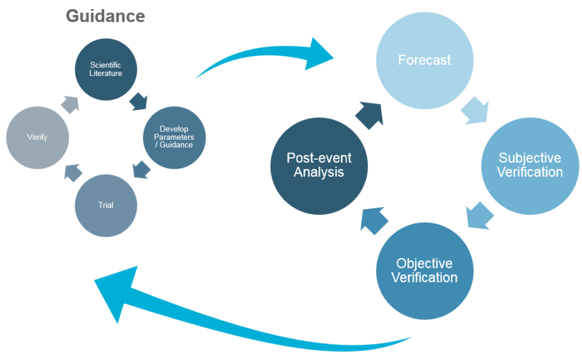

FIG 10: Bureau of Meteorology Extreme Weather Desk end-to-end convection forecast process.

3. THE EXTREME WEATHER DESK CONVECTIVE HAZARD RISK FORECAST PROCESS

The Australian Bureau of Meteorology National Forecast Services' Extreme Weather Desk (EWD), established in May 2015 to provide "a national focus for extreme weather intelligence" and "enhanced severe weather capacity during periods of sustained demand", acts as an operationally orientated testbed for the evaluation and implementation of new scientific approaches, methodologies and NWP. With the goal of improving the diagnosing, forecasting, warning and communication of high-impact convective weather, the EWD developed a complete end-to-end forecast process for convection forecasting (Figure 10) which included the development of guidance systems that inform national hazard risk forecasts of thunder, large hail, damaging wind gusts, heavy rainfall and tornado.

The Day 1 (next day) national hazard risk convection forecasts provide point-based probabilistic forecasts (defined as the probability of lightning, or conditional probability of convective phenomena given a thunderstorm occurring within 10 km of a point) that convey the risk of lightning and severe thunderstorm phenomena which are informed by various sources of guidance.

The graphical forecast risk areas are supplemented by a textual National Convective Outlook Discussion document that provides the evidence-based justifications and reasoning for the forecasts. A strong emphasis is placed on routine verification of the EWD national thunderstorm hazard risk forecasts which consists of daily objective, quantitative and subjective verification and facilitates the continual improvement and bias correction of individual operational meteorologists, the broader EWD team, calibration of guidance systems, and the provision of feedback to research and development.

Guidance is assessed in a cascading format across varying spatial scales, NWP, observational and data frameworks. Beginning with climate to

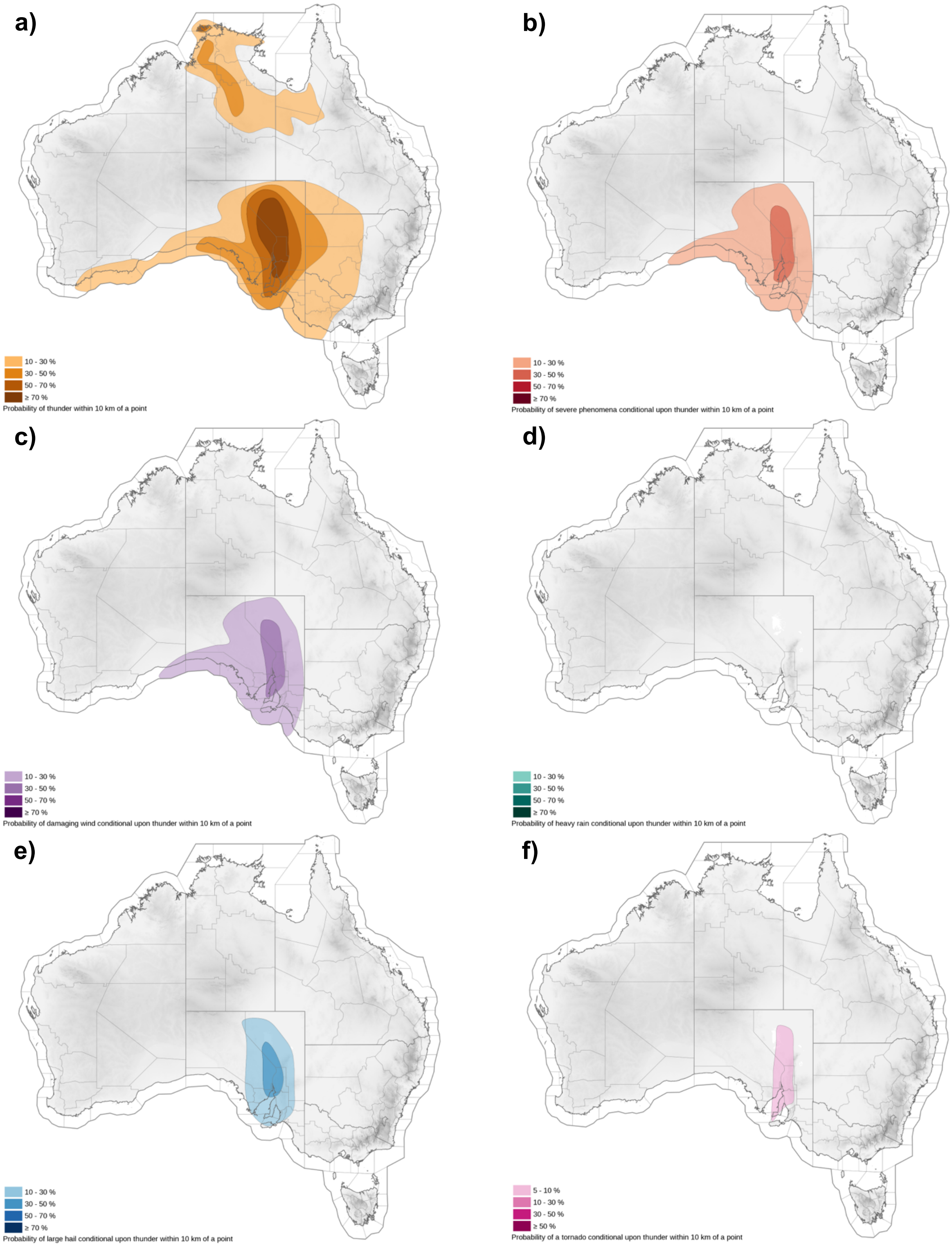

FIG 11. EWD convective hazard risk outlook products issued 27 September 2016, valid 15 UTC 27 – 15 UTC 28 September 2016 depicting the probability within 10 km of a point of a) lightning; b) severe convective phenomena (maximum probability of severe phenomenon) conditional upon lightning; c) damaging convective wind gusts (≥ 90 km h^{-1}) conditional upon lightning; d) heavy convective rainfall (quantitative precipitation accumulation ≥ 10% Annual Exceedance Probability) conditional upon lightning; e) large hail (≥ 2 cm in diameter) conditional upon lightning; and f) tornadoes conditional upon lightning.

hemisphere-scale forcing mechanisms, the Southern Oscillation Index, Madden Julian Oscillation, Indian Ocean Dipole and Southern Annular Mode provide insight into moisture availability, amplification or suppression of downstream systems, and the general pressure and wind regimes. Synoptic-scale interrogation of primarily global or regional parameterized deterministic NWP fields including but not limited to dynamic tropopause (Morgan and Nielsen-Gammon 1998) pressure and wind, potential vorticity (PV) (Davis and Emanuel 1991, Hoskins et al. 1985), cyclonic vorticity advection (CVA) and absolute vorticity (Rowe and Hitchman 2016) are used to assess the dynamical thermodynamic and kinematic forcing mechanisms and their role in enhancing thunderstorm activity. The risk of thunderstorms is assessed via common thermodynamic-based instability parameters of Convective Available Potential Instability (CAPE), Lifted Indices, along with various other instability, lift and moisture fields. Additionally, calibrated thunder (Bright et al. 2005) and the Bureau of Meteorology's National Thunderstorm Forecast Guidance System (Deslandes et al. 2008) are also used to provide first-guess guidance of the probability of lightning occurrence. Convective mode, storm organization and the risk of severe phenomena are assessed using world best practices, methodologies stemming from the scientific literature, and guidance including United States National Weather Service (NWS) Storm Prediction Centre (SPC) normalized convective parameters. The environmental assessment is confirmed or adjusted based upon Convective Allowing Model (CAM) guidance in the form of the Bureau of Meteorology's ACCESS City (Bureau of Meteorology 2018) model domains. Finally, mesoscale analysis is used to assess the real-time environment and potential for severe convective weather which aids short-term communication of convective hazards and warning procedures whilst assisting verification processes.

The primary guidance sources used for the probabilistic convective outlook forecast products issued on 27 September 2016 valid for the 24-hour period of 15 UTC 27 September to 15 UTC 28 September 2016 (15 UTC is considered the universal midnight for Australia) (as illustrated in Figure 11), were the 12 UTC 26 September 2016 runs of the Bureau of Meteorology's ACCESS-R 0.125º regional deterministic model (Bureau of Meteorology 2016a), and the ECMWF (Owens and Hewson 2018) global atmospheric deterministic model (received at 0.125º resolution). Note that real-time CAM guidance was not available for this event.

4. ANTECEDENT CONDITIONS AND CLIMATE FORCING MECHANISMS

Australia experienced its second wettest winter on record in 2016 and the wettest winter for the state of South Australia since 2001 thanks to the combination of positive Southern Oscillation Index (SOI) and the strongest negative Indian Ocean Dipole (IOD) in the preceding 15 years and associated record high sea surface temperatures off the northwest Australian coast. Negative IOD events provide increased available moisture to weather systems traversing the continent which promoted well above average rainfall over Australia during winter and spring. Consequently, the continuation of rainfall events into September resulted in increased soil moisture (highest on record root zone soil moisture deviation from average for 27 September 2016 as illustrated in Figure 12) allowed for enhanced and unseasonable atmospheric moisture availability.

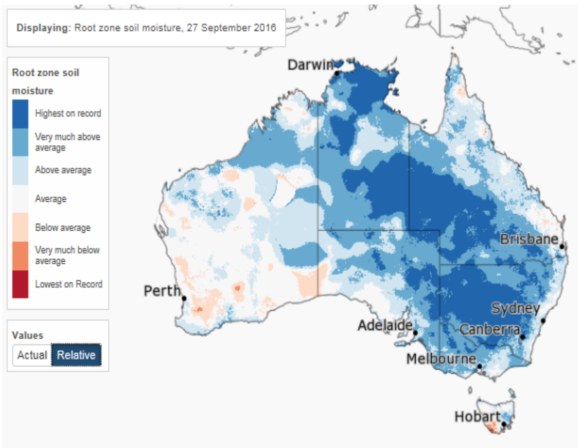

FIG 12: Root zone soil moisture anomalies for 27 September, 2016.

5. SYNOPTIC-SCALE FORCING

Active tropics over southeast Asia in conjunction with an active Madden-Julian Oscillation (MJO) over the eastern Indian Ocean lead to strong ridging over the southern Indian Ocean via the advection of anticyclonic PV (e.g. Parker et al. 2014) which, in turn increased baroclinicity and subsequent strengthening of the polar front jet stream. Coupled with highly mobile synoptic-scale Rossby waves, the approaching wave amplified rapidly south of Western Australia on 27 September before becoming negatively tilted and subsequently over-turning and "breaking" on the 28 September. Explosive cyclogenesis ensued, with the developing low south of the Great Australian Bight deepening by 23 hPa in 24 hours to be 973 hPa during the afternoon of 28 September; Adelaide (South Australia's capital city) recorded its lowest barometric pressure on record (977.3 hPa) as the centre of the mid-latitude cyclone passed to the south of Adelaide during the morning of 29 September. Strong frontogenesis of the fast-moving front extending ahead of the parent low resulted in response to the vertical coupling with strong CVA and the poleward exit region of the sub-tropical jet stream aloft (Figure 13). The front traversed central and eastern South Australia during the afternoon and evening of 28 September, providing the primary lifting mechanism for thunderstorms, the axis of which acted as the focus point of highly

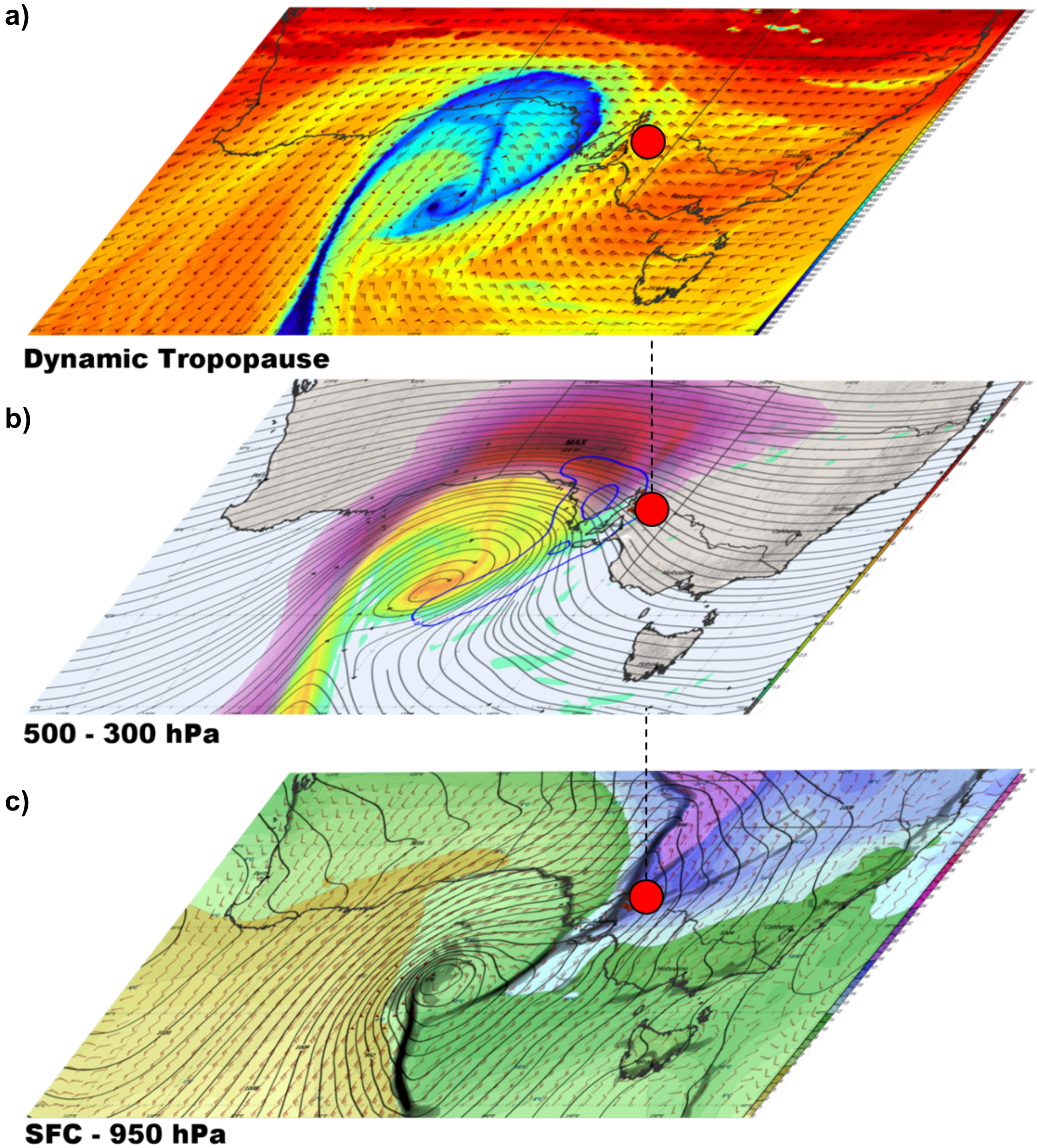

FIG 13. Bureau of Meteorology APS2 ACCESS-R 00 UTC 28 September 2016 run valid 06 UTC a) -1.5 PVU Dynamic Tropopause pressure and wind barbs; b) 500-300 hPa layer mean PV (yellow-green shading), streamlines, CVA (blue contours) and isotachs (purple/red shading) and c) SFC-950hPa layer mean wind barbs, Instantaneous Contraction Rate (grey shading) (Cohen and Schultz 2005), WBPT (color-filled contours), and MSLP (black contours). Red dot indicates broad position of tornado reports

convergent winds stemming from strong pressure and thermodynamic gradients and resultant pre-frontal isallobaric east to northeasterly wind.

6. CONVECTIVE ENVIRONMENT

Severe thunderstorms primarily formed in the warm and humid air mass between the frontogenetic cold front, and warm front to the east that joined at the frontal occlusion to form a triple point within the vicinity of tornado reports (Figure 13c). Based on the 00 UTC 28 September 2016 ACCESS-R model run valid at 06 UTC (nearest forecast time to observed tornado occurrences that depicted the pre-storm environment), the convective environment was characterized by strong pre-frontal moisture advection (3-hr dew point temperature rates of change up to 6°C 3 hr^{-1}) with wet-bulb potential temperatures of 16-18°C leading to strong moisture convergence and the sharpening of the density gradient across the front (cross-frontal mixing ratio gradient of 4 - 5 g kg^{-1}) assisting density related uplift. ML-LCLs typically ranged between 700 and 900 m AGL, with ML-CAPE[2] values rather low ranging between 500 and 1200 J kg^{-1} and ML-CIN values of 20 - 50 J kg^{-1}. The deep layer shear profile was favorable for storm organization consisting of a backing wind profile with height and deep layer bulk wind difference of 50 to 60 kt. Forecast SFC-1 km and SFC-3 km AGL Storm Relative Helicity (SRH) (Davies-Jones 1984) values were generally -150 and -400 $m^2 s^{-2}$ respectively for an unmodified storm motion vector[3] of approximately 340°/35 kt, and -250 and -500 $m^2 s^{-2}$ respectively for Bunkers left moving supercell storm motion vector[4] (Bunkers et al. 2000) of approximately 320°/35 kt suggesting ample streamwise vorticity within the storm inflow layer to support cyclonic supercell organization. This was further supported by Supercell Composite Parameter[5] (SCP) (Thompson et al. 2003) values of 3-4 suggesting that the environment was conducive to supercell organization. Significant Tornado Parameter[6] (STP) (Thompson et al. 2003) values generally ranged between 1 and 2 (Figure 14) within the area of observed tornadoes suggesting an environment conducive to significant (EF2+) tornadoes.

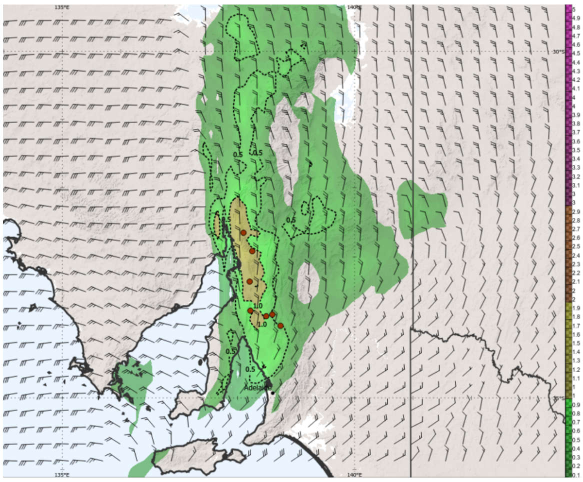

FIG 14: 00 UTC 28 September 2016 ACCESS-R run valid 06 UTC Significant Tornado Parameter (dashed contours at 0.5 intervals) and 10 m AGL wind barbs. Red dots show tornado reports.

7. MESOSCALE ENVIRONMENT

Convective Allowing Model output from the Bureau of Meteorology's 1.5-km resolution APS3 ACCESS-C AD (Adelaide) limited domain model was not available to operational meteorologists at the time of forecast preparation but is presented here to demonstrate how CAM output can be used to confirm the convective environmental assessment obtained from parameterized NWP within the EWD convective forecast process. Nested within the APS2 ACCESS-R 0.125º resolution regional model, the ACCESS-C hindcast was initialized from the ACCESS-R start dump at 03 UTC from the corresponding 00 UTC model run such that, the forecast valid at 06 UTC was a +3-hr forecast.

CAM derived hourly maximum absolute 2-5 km AGL Updraft Helicity (Kain et al. 2008, Kain et al. 2010) accumulated for the period 05-07 UTC (Figure 15a) suggested vigorous rotating updrafts with absolute values reaching >300 $m^2 s^{-2}$ consistent with supercell organization[7] and confirming the assessment that the environment was conducive to rotating thunderstorms.

[2] With virtual temperature correction applied after Doswell and Rasmussen (1994).
[3] Approximated by the 10m AGL - 500 hPa non-pressure weighted mean wind.
[4] Approximated by the unmodified storm motion vector as per [2], 10m AGL - 950 hPa non-pressure weighted mean wind for the tail of the vertical wind shear vector, and 500 hPa wind for the head of the vertical wind shear vector.
[5] The BRN shear term of the SCP was approximated using the bulk wind difference between 10 m AGL and 500 hPa, while the surface-based CAPE was used, and the 0-3 km AGL SRH used an approximated left-moving supercell storm motion vector.
[6] Bulk shear term approximated by the vector wind shear magnitude between 10 m AGL and 500 hPa, and 0-1 km AGL SRH used an approximated left-moving supercell storm motion vector.
[7] Kain et al. (2008) considered an Updraft Helicity threshold of 50 $m^2 s^{-2}$ suitable for the detection of mesocyclones, although Storm Prediction Center (SPC) guidance displays use thresholds of 75 and 150 $m^2 s^{-2}$ (e.g. https://www.spc.noaa.gov/exper/href/index.php) which are arguably better suited for more intense mesocyclones and reduced grid length scales.

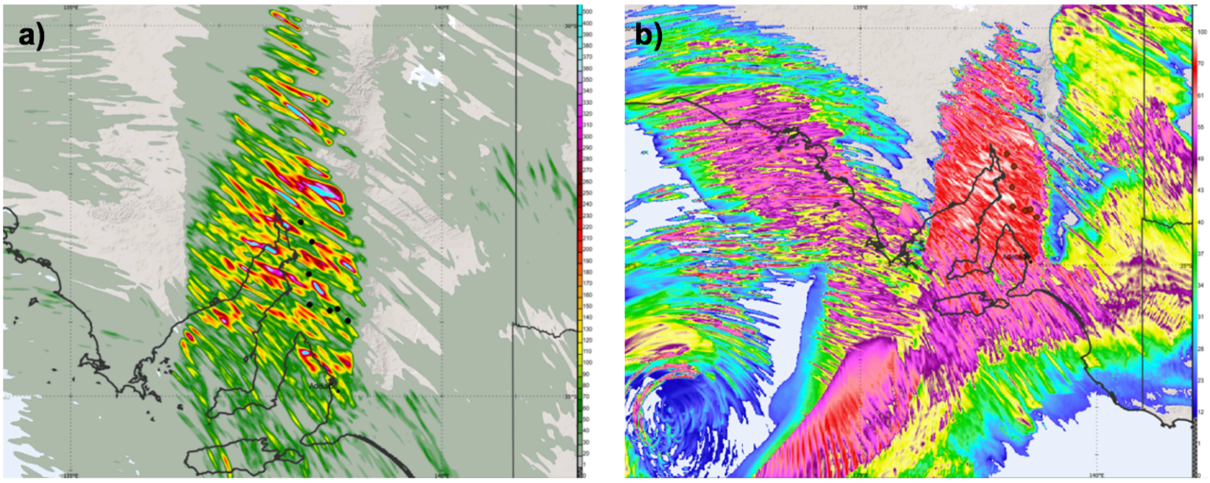

FIG 15. 00 UTC 28 September 2016 ACCESS-C run valid 06 UTC a) maximum 2-5 km AGL Updraught Helicity for the period 05-07 UTC and b) maximum 1 km AGL simulated RADAR reflectivity for the period 05-07 UTC. Dots show tornado reports.

Furthermore, the 1-km AGL hourly maximum simulated RADAR reflectivity accumulated for the period 05-07 UTC (Figure 15b) also indicated intense precipitation simulated reflectivity echoes reaching 60-70 dBZ suggesting the existence of strong convective storms, while confirming the operational meteorologist's assessment of QLCS convective mode.

8. VERIFICATION

The Extreme Weather Desk runs a non-operational mesoanalysis system for demonstration purposes which constructs point-based thermodynamic surface-based or mixed-layer parcels from surface METAR observations which are subsequently ingested into the closest ACCESS-R NWP time step from the latest model run relative to the analysis time. A range of convective parameters and indices are calculated from the point-based constructed thermodynamic profiles and parcels including normalized composite parameters before an objective analysis is performed on a normalized 40 km Cartesian grid. The output of the pseudo-mesoanalysis is output natively within the Bureau of Meteorology's primary data visualization system, Visual Weather by IBL Software Engineering, and via a dedicated proof-of-concept image-based mesoanalysis web-based viewer. The pseudo-mesoanalysis suggested SCP values of 5-10 and STP values of 2-3 (Figure 16) within the area of reported tornadoes at 06 UTC that provided supportive evidence that the environment was conducive to supercell organization and significant tornadoes.

An analysis of the Blyth tornado (situated ~100 km north of Adelaide's Buckland Park S-band RADAR) revealed a 0.5º elevation Doppler maximum rotational velocity of 62 kt at ~1400 m AGL in the vicinity of the reflectivity hook echo signature at 06:01 UTC (Figure 17). When combined with a maximum (within 80 km from the EWD pseudo-mesoanalysis) STP value of 2.7 (Figure 16), the unconditional probability of a tornado after Smith et al. (2015) was ~70%, whilst the combined conditional probability of an EF2+ tornado rating was 40-50% which is consistent with the estimated F2 tornado intensity damage rating for the Blyth tornado obtained via damage assessment.

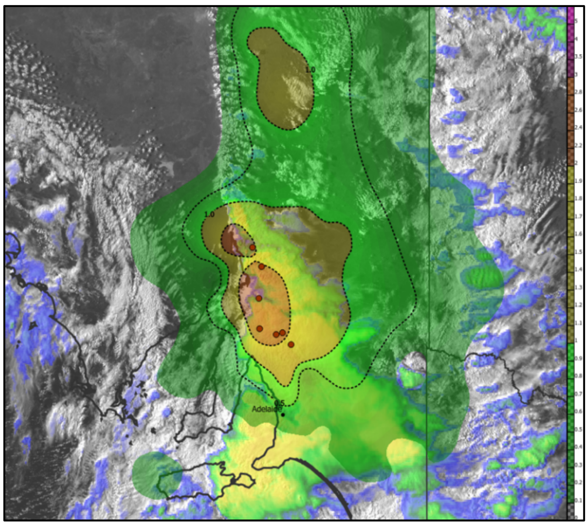

FIG 16. 06 UTC 28 September 2016 STP pseudo-mesoanalysis with red dots showing tornado reports.

Hodograph analysis of the Adelaide Airport 04:40 UTC atmospheric profile (Figure 18) with observed 0615 UTC pre-storm winds substituted from Clare (situated 11 km southeast of Blyth) of 040º/15 kt and an observed storm motion vector of 320º/41 kt (closely approximated by the ACCESS-R 00 UTC run valid at 06 UTC 28 September 2016 derived Bunkers left storm motion vector of 320°/35 kt) resulted in SFC-1 km and SFC-3 km AGL SRH values of -845 $m^2 s^{-2}$ and -1094 $m^2 s^{-2}$ respectively. With 10 m - 500 m AGL shear of 38 kt and 10 m AGL storm relative inflow of 119º/41 kt, the Tornado Critical Angle, which has been shown to be a strong discriminator between tornadic and non-tornadic supercells by Esterheld and Giuliano (2008), was found to be 87º, suggesting the ingestion of nearly pure streamwise vorticity concentrated in the near-surface storm inflow layer. This promotes a stronger low-level mesocyclone and subsequent increased vertical vortex stretching via dynamic lifting, favoring tornadogenesis (Coffer and Parker 2017).

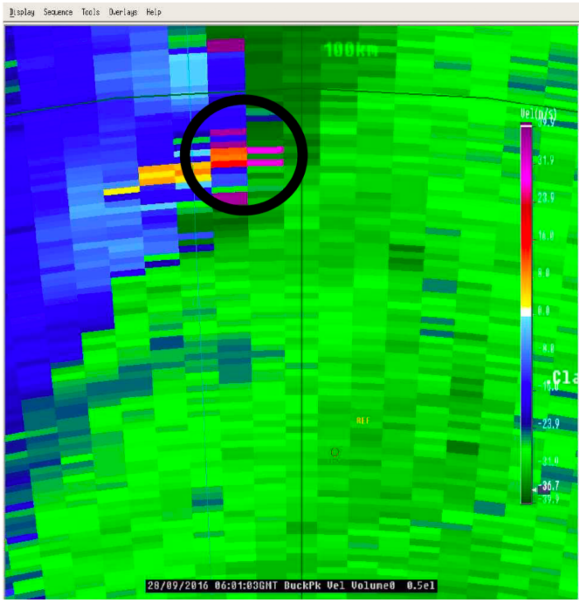

FIG 17. Buckland Park Doppler Radar 0.5° elevation velocity scan at 06:01 UTC of the supercell thunderstorm responsible for the Blyth tornado with a peak rotational velocity is 62 kt (circled in black) at a height of 1400 m AGL.

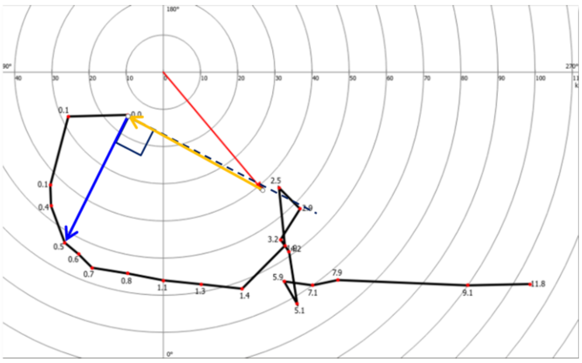

FIG 18. Adelaide Airport (YPAD) 04:40 UTC hodograph with observed storm motion vector (red), storm relative inflow vector (orange) and 10-500 m AGL shear vector (blue).

As part of the end-to-end convective hazard risk forecast process, the EWD calculates daily objective spatial verification of the probabilistic convective outlook for lightning, although this was not available to EWD operational meteorologists at the time. The probabilistic forecast for lightning for this event (Figure 19) verified well with observed spatial coverages close to or within forecast spatial coverages. The probabilistic forecasts of severe convective phenomena cannot be verified objectively due to the sparseness of observations, although in this case, all tornado reports resided within the 5% conditional probability risk area for tornadoes. Routine daily objective, quantitative and subjective verification in the EWD facilitates the continual improvement and bias correction of individual operational meteorologists and the broader EWD team.

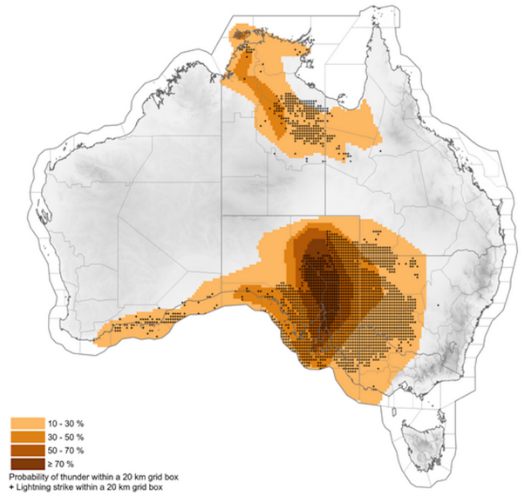

Forecast Probability	Grid Points Forecast	Fractional Area Forecast	Grid Points with Lightning	Observed Coverage
0-10%	16537	73.7%	51	0.3%
10-30%	3903	17.4%	1040	26.6%
30-50%	1243	5.5%	668	53.7%
50-70%	414	1.8%	295	71.3%
>70%	346	1.5%	274	79.2%
			Brier Score:	0.065

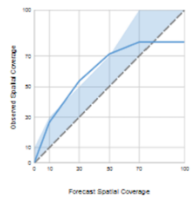

FIG 19. EWD objective spatial verification of the Day 1 (next day) probabilistic convective hazard risk forecast valid 28 September 2016.

9. CONCLUSION

Guidance systems implemented within the EWD's end-to-end convective forecast process which includes NWS SPC normalised convective parameters were useful in diagnosing and highlighting environments conducive to tornadic supercell thunderstorms and demonstrated their application in the Southern Hemisphere. CAM guidance and pseudo-mesoanalysis, if utilized operationally for short-term forecasts and warnings, can be used to confirm the convective environmental assessment and increase confidence in convective mode and probabilistic convective forecasts, allowing for refined probabilities to be forecast for convective threats and improve the communication of high-impact convective hazards.

The EWD's probabilistic convective hazard risk forecasts successfully conveyed the convective hazard risk of lightning and severe convective phenomena. Objective spatial verification of the EWD's convective hazard risk forecast product for lightning verified well, while all tornado reports resided within the conditional tornado probability risk area. Additionally, the combination of RADAR observations and pseudo-mesoanalysis of STP provided further supportive evidence for the occurrence of tornadoes.

Acknowledgements. Special thanks and appreciation are extended to Susan Rennie (Bureau of Meteorology) for running the hindcast APS3 ACCESS-C (AD) CAM NWP model and making the data available to the EWD; Peter Steinle and Charmaine Franklin (Bureau of Meteorology) for providing insight into NWP configurations; Harald Richter (Bureau of Meteorology) for the input, guidance, support and implementation of calibrated thunder within the Bureau of Meteorology; and the South Australia state office administration staff for assistance with logistical and budget support activities to enable the damage assessment.

We further wish to recognize the support provided by the National Forecast Services and Extreme Weather Desk teams, and in particular the contributions by EWD and South Australia state office operational meteorologists.

REFERENCES

Australian Bureau of Statistics, 2018: Australian Demographic Statistics, Sep 2017, cat. no. 3101.0. Accessed 22 March 2018, http://www.abs.gov.au/AUSSTATS/abs@.nsf/Lookup/3101.0Main+Features1Sep%202017?OpenDocument.

Bureau of Meteorology, 2016a: BNOC Operations Bulletin Number 107 - PS2 Upgrade to the ACCESS-R Numerical Weather Prediction System. 29pp, http://www.bom.gov.au/australia/charts/bulletins/apob107-external.pdf

Bureau of Meteorology, 2016b: Severe thunderstorm and tornado outbreak South Australia 28 September 2016. 54pp, http://www.bom.gov.au/announcements/sevwx/sa/Severe_Thunderstorm_and_Tornado_Outbreak_28_September_2016.pdf.

Bureau of Meteorology, 2018: NOC Operations Bulletin Number 114 - APS2 upgrade of the ACCESS-C Numerical Weather Prediction system. 33pp, http://www.bom.gov.au/australia/charts/bulletins/BNOC_Operations_Bulletin_114.pdf

Australian Energy Market Operator Ltd., 2016: Preliminary Report – Black System Event in South Australia on 28 September 2016. 41pp.

Australian Energy Market Operator Ltd., 2017: Black System South Australia 28 September 2016 – Final Report. 271pp, https://www.aemo.com.au/-/media/Files/Electricity/NEM/Market_Notices_and_Events/Power_System_Incident_Reports/2017/Integrated-Final-Report-SA-Black-System-28-September-2016.pdf

Bright, D. R., M. S. Wandishin, R. E. Jewell, and S. J. Weiss, 2004: A physically based parameter for lightning prediction and its calibration in ensemble forecasts. Preprints, *Conf. on Meteor. Appl. of Lightning Data, Amer. Meteor. Soc., San Diego, CA*, **3496**, 30.

Bunkers, M. J., B. A. Klimowski, J. W. Zeitler, R. L. Thompson, and M.L. Weisman, 2000: Predicting supercell motion using a new hodograph technique. *Wea. Forecasting*, **15(1)**, 61-79, https://doi.org/10.1175/1520-0434(2000)015<0061:PSMUAN>2.0.CO;2.

Coffer, B. E., and M. D. Parker, 2017: Simulated supercells in nontornadic and tornadic VORTEX2 environments. *Mon. Wea. Rev.*, **145(1)**, 149-180, https://doi.org/10.1175/MWR-D-16-0226.1.

Cohen, R. A., and D. M. Schultz, 2005: Contraction rate and its relationship to frontogenesis, the Lyapunov exponent, fluid trapping, and airstream boundaries. *Mon. Wea. Rev.*, **133(5)**, 1353-1369, https://doi.org/10.1175/MWR2922.1.

Davies-Jones, R., 1984: Streamwise vorticity: The origin of updraft rotation in supercell storms. *J. Atmos. Sci.*, **41(20)**, 2991-3006, https://doi.org/10.1175/1520-0469(1984)041<2991:SVTOOU>2.0.CO;2.

Davis, C. A., and K. A. Emanuel, 1991: Potential vorticity diagnostics of cyclogenesis. *Mon. Wea. Rev.*, **119(8)**, 1929-1953, https://doi.org/10.1175/1520-0493(1991)119<1929:PVDOC>2.0.CO;2.

Deslandes, R., H. Richter, and T. Bannister, 2008: The end-to-end severe thunderstorm forecasting system in Australia: overview and training issues. *Australian Meteorological Magazine*, **57(4)**, https://pdfs.semanticscholar.org/a694/5ed4777f2558103c140204a1d788827cadae.pdf.

Doswell III, C. A., and E. N. Rasmussen, 1994: The effect of neglecting the virtual temperature correction on CAPE calculations. *Wea. Forecasting*, **9(4)**, 625-629, https://doi.org/10.1175/1520-0434(1994)009<0625:TEONTV>2.0.CO;2.

Esterheld, J. M. and D. J. Giuliano, 2008: Discriminating between tornadic and non-tornadic supercells: A new hodograph technique. *E-Journal of Severe Storms Meteorology*, **3(2)**, http://www.ejssm.org/ojs/index.php/ejssm/article/download/33/38

Fujita, T.T., 1981: Tornadoes and downbursts in the context of generalized planetary scales. *J. Atmos. Sci.*, **38**, 1511-1534.

Hoskins, B. J., M. E. McIntyre, and A. W. Robertson, 1985: On the use and significance of isentropic potential vorticity maps. *Quarterly Journal of the Royal Meteorological Society*, **111(470)**, 877-946, https://doi.org/10.1002/qj.49711147002.

Kain, J. S., and Coauthors, 2008: Some practical considerations regarding horizontal resolution in the first generation of operational convection-allowing NWP. *Wea. Forecasting*, **23**, 931–952, https://doi.org/10.1175/WAF2007106.1.

Kain, J. S., S. R. Dembek, S. J. Weiss, J. L. Case, J. J. Levit, and R. A. Sobash, 2010: Extracting unique information from high-resolution forecast models: Monitoring selected fields and phenomena every time step. *Wea. Forecasting*, **25**, 1536–1542, https://doi.org/10.1175/2010WAF2222430.1.

McDonald, J. and K. C. Mehta, 2006: A Recommendation for an Enhanced Fujita Scale (EF-Scale), Revision 2. Wind Science and Engineering Research Center, Texas Tech University, Lubbock, TX, 111 pp.

Morgan, M. C., and J. W. Nielsen-Gammon, 1998: Using tropopause maps to diagnose midlatitude weather systems. *Mon. Wea. Rev.*, **126(10)**, 2555-2579, https://doi.org/10.1175/1520-0493(1998)126<2555:UTMTDM>2.0.CO;2.

Owens, R.G., and T.D. Hewson, 2018: ECMWF Forecast User Guide. ECMWF, Accessed 20 November 2018. doi:10.21957/m1cs7h, https://confluence.ecmwf.int/display/FUG/Forecast+User+Guide.

Parker, T. J., G. J. Berry, and M. J. Reeder, 2014: The structure and evolution of heat waves in southeastern Australia. *Journal of Climate*, **27(15)**, 5768-5785, https://doi.org/10.1175/JCLI-D-13-00740.1.

Rowe, S. M., and M. H. Hitchman, 2016: On the relationship between inertial instability, poleward momentum surges, and jet intensifications near midlatitude cyclones. *J. Atmos. Sci.*, **73(6)**, 2299-2315, https://doi.org/10.1175/JAS-D-15-0183.1.

Smith, B. T., R. L. Thompson, A. R. Dean, and P. T. Marsh, 2015: Diagnosing the conditional probability of tornado damage rating using environmental and radar attributes. *Wea. Forecasting*, **30(4)**, 914-932, https://doi.org/10.1175/WAF-D-14-00122.1.

Thompson, R. L., R. Edwards, J. A. Hart, K. L. Elmore, and P. Markowski, 2003: Close proximity soundings within supercell environments obtained from the Rapid Update Cycle. *Wea. Forecasting*, **18(6)**, 1243-1261, https://doi.org/10.1175/1520-0434(2003)018<1243:CPSWSE>2.0.CO;2.